Chemical short-range order and lattice deformations in $Mg_yTi_{1-y}H_x$ thin films probed by hydrogenography

R. Gremaud,[1,*] A. Baldi,[1] M. Gonzalez-Silveira,[1] B. Dam,[1] and R. Griessen[1]
[1]*Faculty of Sciences, Department of Physics and Astronomy, Condensed Matter Physics, VU University Amsterdam, De Boelelaan 1081, 1081 HV Amsterdam, The Netherlands*
(Received 5 February 2008; published 8 April 2008)

A multisite lattice gas approach is used to model pressure–optical-transmission isotherms (PTIs) recorded by hydrogenography on $Mg_yTi_{1-y}H_x$ sputtered thin films. The model reproduces the measured PTIs well and allows us to determine the chemical short-range order parameter s. The s values are in good agreement with those determined from extended x-ray absorption fine structure measurements. Additionally, the PTI multisite modeling yields a parameter L that accounts for the local lattice deformations with respect to the average Mg_yTi_{1-y} lattice given by Vegard's law. It is thus possible to extract two essential characteristics of a metastable alloy from hydrogenographic data.

DOI: 10.1103/PhysRevB.77.144204 PACS number(s): 63.50.Gh, 64.60.A−, 64.75.Op

I. INTRODUCTION

Mg and Ti are considered as immiscible, as their enthalpy of mixing is positive ($\Delta H_{\mathrm{mix}} > 20$ kJ/mol atom).[1] Alloying of Mg and Ti does, however, take place in mechanically alloyed bulk samples,[2] in physical vapor deposition,[3] e-beam deposition,[4,5] and sputtering of thin films.[6–8] In general, understanding the degree of mixing achievable in immiscible systems is of considerable scientific and technological interest.[9–12] In particular, the fact that reproducible and reversible switching from metal to hydride without noticeable segregation of the metal constituents occurs in Mg-Ti thin films[8] makes it an even more fascinating model system to study.

Continuous monitoring of the structure during H uptake by x-ray diffraction (XRD) hints at a persistent coherent structure during the whole (de)hydrogenation process. Additional electrical and spectrophotometric measurements suggest that Mg-Ti films are structurally coherent at the XRD scale but locally partially chemically segregated.[8] It is thus of interest to probe how much decomposition has occurred and on what spatial scale.

Thanks to their peculiar structural properties, Mg-Ti-H thin films are also of interest for application as optical switchable devices, e.g., for solar collectors[6,13] and fiber optic hydrogen sensors.[14] While metallic in the as-deposited state (high optical reflectance and very low optical transmittance), the films become highly absorbing (low reflectance and transmittance) upon hydrogen uptake. The high degree of mixing between Mg and Ti in sputtered films is directly responsible, via a lowering of the plasma frequency,[15] for an unusual "black" optical state. The optical change in optical transmission upon hydrogen absorption makes $Mg_yTi_{1-y}H_x$ thin films also ideally suited for hydrogenography, a high-throughput combinatorial method for the search of new lightweight hydrogen storage materials.[16,17] This technique makes it possible to measure pressure–*optical transmission* isotherms (PTIs) on hydrides with a metal-to-semiconductor transition,[16] as well as on hydrides that remain metallic upon hydrogenation.[17] From Lambert–Beer's law, $\ln(T/T_M)$, the logarithm of the optical transmission T in a film of initial transmission T_M, is expected to linearly vary with the hydrogen concentration.[18] This is confirmed by joint electrochemical and optical measurements.[8] The obtained PTIs are therefore fully analogous to pressure-concentration isotherms (PCI) obtained with standard volumetric or gravimetric methods.[17]

The formation enthalpy of bulk TiH_2 [$\Delta H = -130$ kJ $(\mathrm{mol\ H_2})^{-1}$] is almost twice as negative as the one of bulk MgH_2 [$\Delta H = -76$ kJ $(\mathrm{mol\ H_2})^{-1}$].[19] In a fully segregated sample, one would therefore expect Ti to form a hydride at lower pressures than Mg in the film, resulting in two well-defined plateaus in the PTIs. However, both PTIs[16] and electrochemical isotherms[4] of Mg_yTi_{1-y} thin films present an unusual shape that is not compatible with a sequential formation of TiH_2 and MgH_2.

In this paper, we present a multisite lattice gas model for optical isotherms and apply it on PTIs measured by hydrogenography on $Mg_yTi_{1-y}H_x$ sputtered thin films. The model reproduces the measured PTIs well and allows us to derive experimental values of the chemical short-range order parameter (CSRO) s which are in good agreement with the local surrounding of Ti and s values determined by extended x-ray absorption fine structure (EXAFS).[20] Furthermore, the model gives information on the local lattice's departures from the average lattice given by Vegard's law.

II. EXPERIMENT

A. Sample preparation

Mg_yTi_{1-y} thin films with a compositional gradient are prepared in a seven-gun ultrahigh-vacuum dc/rf magnetron cosputtering system (base pressure of 10^{-7} Pa) at room temperature on 70×5 mm^2 quartz substrates. Mg and Ti are facing each other in tilted off-axis sputtering guns. By adjusting the power applied to each gun, the desired compositional region of the binary phase diagram is obtained. The local composition of the gradient films is determined by Rutherford backscattering spectrometry on films grown in the same deposition run on amorphous carbon substrates. The Mg atomic fraction y along the length of the sample varies

between 0.6 and 0.89. All the films with thickness of 30–100 nm are covered *in situ* with a 20 nm Pd cap layer to promote H_2 dissociation and to prevent oxidation of the underlying film.

B. Data collection

After deposition, metallic films are transferred into an optical cell to monitor their optical transmission during hydrogenation.[18] The whole cell is placed in an oven to control the temperature up to 300 °C. A 150 W diffuse white light source illuminates the sample from the substrate side and a three-channel (RGB) Sony XC-003 charged-coupled device camera continuously monitors the transmitted light as a function of hydrogen pressure. The three-channel transmission intensities are added, resulting in a 1.1–3.3 eV photon energy bandwidth. More information about the PTI acquisition can be found in Ref. 16.

For the determination of optical absorption coefficients, spectrophotometric reflection and transmission measurements of Mg and Ti in the metallic and hydrogenated states are performed in a Perkin Elmer Lambda 900 diffraction grating spectrometer with an energy range from 0.495 to 6.19 eV (wavelength $\lambda=2500-200$ nm).

III. EXPERIMENTAL PRESSURE–OPTICAL-TRANSMISSION ISOTHERMS

Figure 1 shows various PTIs of Mg_yTi_{1-y} with $0.61 \leqslant y \leqslant 0.85$ at temperature $\mathcal{T}=363$ K. The average coherent structure determined by XRD and plan view transmission electron microscopy is hcp in the metallic state and fcc in the hydrided state.[8] Compositions with $y>0.85$ are not considered here because of the presence of rutile MgH_2 that coexists with the fcc structure. The dashed lines indicate the transmission in the metallic state T_M for the various compositions. For all compositions, the optical transmission T increases with increasing hydrogen pressure. Starting from low pressures, the transmission first increases gradually, and then a sloping plateau develops at a higher pressure. The plateau shifts toward higher pressures and widens with increasing Mg atomic fraction y. Conversely, the gradual transmission increase with pressure is the dominant feature in the isotherms for the Ti-richest compositions ($0.61 \leqslant y < 0.7$). We show in the following that this PTI shape evolution with Mg fraction y is neither compatible with randomly distributed Mg and Ti atoms nor with completely phase segregated Mg and Ti (hydride) phases.

IV. PRESSURE–OPTICAL TRANSMISSION ISOTHERM MODELING: LATTICE GAS MODEL FOR H IN A MULTISITE SOLID WITH LONG-RANGE H-H INTERACTION

In this section, we show that a multisite lattice gas model[21–23] with tetrahedral interstitial sites Mg_jTi_{4-j} ($0 \leqslant j \leqslant 4$) including chemical short-range order[24,25] is suitable to model the PTIs. The six essential ingredients of the multisite lattice gas model are the following:

(1) types and fractions of the various interstitial sites,

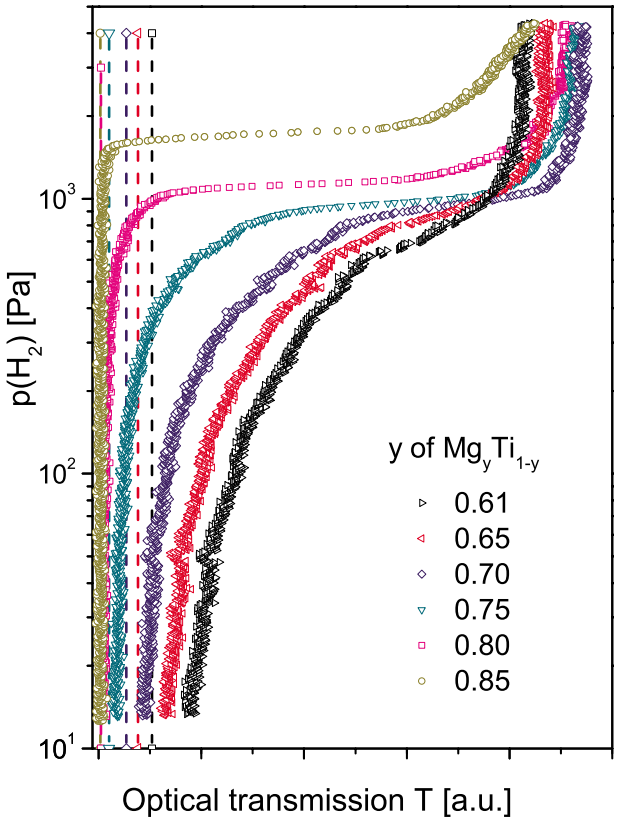

FIG. 1. (Color online) Pressure–optical-transmission isotherms at $\mathcal{T}=363$ K of a thin Mg_yTi_{1-y} film with a continuous gradient in alloy composition. Dashed lines indicate the transmission in the metallic state T_M.

(2) local lattice deformation of the host lattice due to alloying of Mg and Ti,

(3) enthalpy of hydrogen solution for each site type,

(4) degree of occupation of interstitial sites at thermodynamic equilibrium with the surrounding H_2 gas,

(5) long-range H-H interaction in the lattice gas, and the

(6) relation between the total hydrogen concentration and the optical transmission.

A. Mg-Ti interstitial sites: Types and fractions

The as-deposited Mg_yTi_{1-y} films are neither perfectly random nor fully segregated.[20] To characterize their overall degree of chemical segregation as a function of composition y, we use the CSRO parameter defined as[26]

$$s = 1 - \frac{N_{BA}}{Ny}, \tag{1}$$

for a A_yB_{1-y} system, where N_{BA} is the nearest neighbor coordination number of A atoms around a B atom (here, $A=$Mg and $B=$Ti), N is the total coordination number in the nearest neighbor shell, and y is the atomic fraction of A. Positive, zero, and negative CSRO parameters indicate clustered, random, and ordered spatial distributions of atoms, respectively.

We assume that H in a Mg_yTi_{1-y} alloy can occupy tetrahedral interstitial sites Mg_jTi_{4-j} with $0 \leqslant j \leqslant 4$. There are N_j

sites of type j and the total number of sites is $N=\Sigma_j N_j$. By using a chain model[24] to calculate the fraction $g_j=N_j/N$ of each hydrogen site type, we obtain the following relations:

$$g_0=(1-y)(1-y+ys)^3, \tag{2}$$

$$g_1=2(1-y)(1-y+ys)^2y(1-s)+2(1-y)^2(1-y+ys)y(1-s)^2, \tag{3}$$

$$g_2=2(1-y)(1-y+ys)y(1-s)[y+(1-y)s]+2(1-y)^2y^2(1-s)^3+(1-y)^2y(1-s)^2[y+(1-y)s]+y^2(1-y+ys)(1-s)^2(1-y), \tag{4}$$

$$g_3=2(1-y)y(1-s)[y+(1-y)s]^2+2y^2(1-s)^2(1-y)[y+(1-y)s], \tag{5}$$

$$g_4=y[y+(1-y)s]^3, \tag{6}$$

for Ti_4, $MgTi_3$, Mg_2Ti_2, Mg_3Ti, and Mg_4 sites, respectively, with, of course, $\Sigma_j g_j=1$.

B. Local lattice deformations due to alloying

Magnesium has a larger molar volume than Ti ($V_{Mg}=13.97$ cm^3/mol, $V_{Ti}=10.64$ cm^3/mol). This implies that a titanium inclusion in a Mg matrix is somewhat expanded while the Mg matrix is compressed compared to their pure metal volumes.[27] The same applies to clusters of type j. The volume V_j^e of a cluster *embedded* in the alloy matrix is related to the volume V_j^f of a *free* cluster as[24]

$$V_j^e(y)=(1-L)V_{\text{metal}}(y)+LV_j^f, \tag{7}$$

where

$$V_j^f=\frac{jV_{Mg}+(4-j)V_{Ti}}{4}, \tag{8}$$

$$V_{\text{metal}}(y)=yV_{Mg}+(1-y)V_{Ti}, \tag{9}$$

and $V_{Mg,Ti}$ are the molar volumes of the elements. The parameter L accounts for the degree of local deformation of a cluster embedded in an alloy. The meaning of the parameter L is best explained by taking the perfect average crystal with a molar volume $V_{\text{metal}}(y)$ given by Vegard's law [see Eq. (9)]. In this hypothetical perfect lattice, all clusters have the same volume. This corresponds to $L=0$. A positive value for L implies that a Mg-rich cluster is slightly compressed, while a Ti-rich cluster is slightly expanded with respect to the $L=0$ case in an alloy with a coherent lattice but locally modulated lattice spacings. To illustrate the effect of extreme L values, we consider the case of a Mg_4 cluster: in the rigid limit, $L=1$, a Mg_4 cluster keeps the same volume as in pure Mg, while for $L=0$, it is compressed according to the overall composition of the Mg_yTi_{1-y} metal alloy. Note that Vegard's law still applies to the long-range average lattice for all L values.

C. Site dependent enthalpies of hydrogen solution

In the simplest approximation, the enthalpies of hydrogen solution (i.e. for hydrogen concentrations $c\to 0$), $\Delta H_j^{0,f}$ for isolated *free* Mg_jTi_{4-j} clusters are taken as the weighted averages of the hydrogen solution enthalpies ΔH_{Mg}^0 and ΔH_{Ti}^0 in pure Mg and Ti,[22,28]

$$\Delta H_j^{0,f}=\frac{j\Delta H_{Mg}^0+(4-j)\Delta H_{Ti}^0}{4}. \tag{10}$$

For a Mg_jTi_{4-j} cluster embedded in a Mg_yTi_{1-y} matrix, $\Delta H_j^{0,f}$ needs to be corrected for local deformations due to alloying.

Thermodynamically, the volume dependence of the enthalpy of hydride formation is given by[29]

$$\frac{d\Delta H}{d\ln V}=-B(y)V_H(y), \tag{11}$$

where $B(y)$ is the bulk modulus of the alloy,

$$V_H(y)=\frac{V_{\text{dihydride}}(y)-V_{\text{metal}}(y)}{2} \tag{12}$$

is the partial molar volume of H in the alloy,

$$V_{\text{dihydride}}(y)=yV_{MgH_2}+(1-y)V_{TiH_2}, \tag{13}$$

and V_{MgH_2} and V_{TiH_2} are the molar volumes of the dihydrides.

By using Eq. (11), the enthalpy of hydrogen solution for embedded clusters becomes

$$\Delta H_j^{0,e}\simeq\Delta H_j^{0,f}+\frac{d\Delta H^0}{d\ln V}\frac{(V_j^e-V_j^f)}{V_j^f}=\Delta H_j^{0,f}-B(y)V_H(y)\frac{V_j^e(y)-V_j^f}{V_j^f}. \tag{14}$$

The bulk modulus $B(y)$ is taken as the weighted average of the bulk moduli of the metal constituents,

$$B(y)=yB_{Mg}+(1-y)B_{Ti}. \tag{15}$$

D. Occupation of the interstitial sites

With increasing hydrogen pressure, hydrogen gradually fills interstitial sites in the Mg_yTi_{1-y} alloy, starting with sites with the lowest enthalpy, in our case Ti_4 sites. The total number of hydrogen atoms absorbed at a certain hydrogen gas pressure p and temperature $\mathcal{T}$ is denoted by N^H, and the number of hydrogen atoms occupying a given site type by N_j^H. Consequently, the fraction x_j of interstitial site j occupied by hydrogen atoms is

$$x_j=\frac{N_j^H}{N_j}, \tag{16}$$

and the normalized total hydrogen concentration c ($0\leqslant c\leqslant 1$) is

$$c=\frac{N^H}{N}=\sum_{j=0}^{4}\frac{N_j}{N}\frac{N_j^H}{N_j}=\sum_{j=0}^{4}g_jx_j \tag{17}$$

Thermodynamic equilibrium between hydrogen gas and hydrogen at each interstitial site requires that

$$\frac{1}{2}\mu_{H_2}(p,\mathcal{T}) = \mu_H^j(p,\mathcal{T},x_j,c), \quad j=0,\ldots,4, \tag{18}$$

where the chemical potential of H_2 gas is[30]

$$\mu_{H_2} = R\mathcal{T}\left[\ln\left(\frac{p}{p_0}\right) - \frac{S_{H_2}^0}{R}\right] + E_{H_2}, \tag{19}$$

where $S_0=130.68$ J K^{-1} (mol H_2)$^{-1}$ is the entropy of H_2 gas at standard pressure $p_0=1.013\times10^5$ Pa, E_{H_2} is the binding energy of the H_2 molecule, and R is the gas constant.

The chemical potential of H at each interstitial site type can be written as

$$\mu_H^j = R\mathcal{T}\ln\left(\frac{x_j}{1-x_j}\right) + E_j(c), \quad j=0,\ldots,4, \tag{20}$$

where the energy $E_j(c)$ of H at the interstitial site Mg_jTi_{4-j} depends, in general, on the *total* hydrogen concentration c. This is a direct consequence of the infinite range of the elastic H-H interaction in metal hydrides.[31]

By solving Eq. (18) for x_j, one obtains, together with Eq. (17),

$$c = \frac{N^H}{N} = \sum_{j=0}^{4} g_j x_j = \sum_{j=0}^{4} \frac{g_j}{\exp\left\{\dfrac{\Delta H_j(c)}{R\mathcal{T}} - \dfrac{1}{2}\left[\ln\left(\dfrac{p}{p_0}\right) - \dfrac{S_{H_2}^0}{R}\right]\right\} + 1}, \tag{21}$$

with

$$\Delta H_j(c) = E_j(c) - \frac{1}{2}E_{H_2}, \tag{22}$$

which is the concentration dependent enthalpy for H absorption in site j. Equation (21) is a self-consistent equation for $p=p(c)$ that is numerically solved to determine the PCI at temperature $\mathcal{T}$.

E. H-H interaction

In order to calculate $\Delta H_j(c)$, the H-induced lattice expansion has to be taken into account. Increasing the H concentration makes all interstitial sites more favorable for hydrogen[32] and results in an infinite range attractive H-H interaction.[33,34] The contribution of this H-H interaction to the enthalpy of formation is to lowest order given by [see Eq. (11)][25]

$$\Delta H_j(c) \simeq \Delta H_j^{0,e} + \frac{d\Delta H}{d\ln V}\frac{d\ln V}{dc}c = \Delta H_j^{0,e} - B(y,c)V_H(y)\frac{V_{dihydride}-V_{metal}}{2V_{metal}}c, \tag{23}$$

with

$$B(y,c) = y[cB_{MgH_2} + (1-c)B_{Mg}] + (1-y)[cB_{TiH_2} + (1-c)B_{Ti}]. \tag{24}$$

Together with Eq. (14), the enthalpy of hydride formation at a site j becomes

$$\Delta H_j(c) \simeq \Delta H_j^{0,f} - B(y,0)V_H(y)\frac{V_j^e(y)-V_j^f}{V_j^f} - B(y,c)\frac{V_H(y)^2}{V_{metal}}c. \tag{25}$$

The second and third terms in Eq. (25) describe the influence on the enthalpy of formation of local lattice deformations at zero hydrogen concentration and of the filling of sites with hydrogen, respectively.

F. Optical transmission

Lambert–Beer's law is used to calculate the optical transmission T,

$$T = T_0\prod_{j=0}^{4}\exp\{[-\alpha_j^M(1-x_j) - \alpha_j^{MH}x_j]g_j\}, \tag{26}$$

where T_0 is the light intensity in the absence of the sample and $\alpha_j^{M(H)}$ are the optical absorption coefficients of the metallic and hydrided Mg_jTi_{1-j} clusters averaged over the measured photon-energy $\hbar\omega$ bandwidth, respectively. According to Eq. (26), the transmission in the metallic state T_M is

$$T_M = T_0\prod_{j=0}^{4}\exp(-\alpha_j^M g_j). \tag{27}$$

By combining Eqs. (26) and (27), the logarithm of the optical transmission normalized by the transmission in the metallic state is

$$\ln\left(\frac{T}{T_M}\right) = -\sum_{j=0}^{4}(\alpha_j^{MH} - \alpha_j^M)x_j g_j. \tag{28}$$

If the optical change $\alpha_j^{MH}-\alpha_j^M$ was independent of j, i.e., of the cluster composition, then

$$\ln\left(\frac{T}{T_M}\right) \propto c. \tag{29}$$

This is, however, certainly not the case, as MgH_2 is a transparent insulator and TiH_2 is a metal. The simplest approximation would be to neglect the optical change of the metal and take

$$\alpha_j^{MH} - \alpha_j^M \cong j(\alpha_{MgH_2} - \alpha_{Mg}), \tag{30}$$

then

$$\ln\left(\frac{T}{T_M}\right) \cong -(\alpha_{MgH_2} - \alpha_{Mg})\sum_{j=0}^{4} j x_j g_j. \tag{31}$$

This shows that Mg-rich clusters have a predominant contribution to the optical transmission.

The last step is to combine Eqs. (21) and (28) to obtain

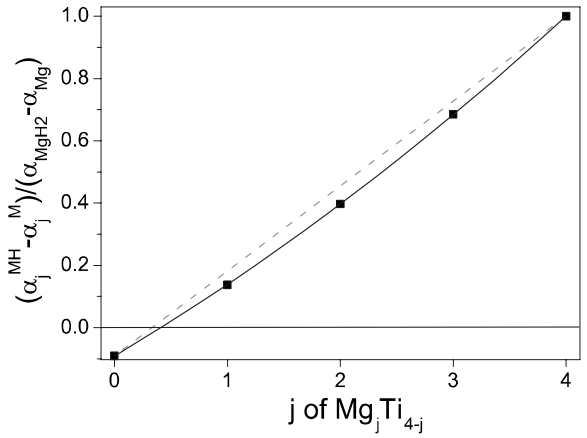

FIG. 2. Squares, normalized absorption coefficient differences of the Mg_jTi_{4-j} clusters obtained by density functional theory (Ref. 15) used in the PTI simulations. Dashed line, linear interpolation between the Mg and Ti values. The black line is a guide to the eyes.

$$\ln\left(\frac{T}{T_M}\right)=\sum_{j=0}^{4}\frac{(\alpha_j^M-\alpha_j^{MH})g_j}{\exp\left\{\frac{\Delta H_j(c)}{R\mathcal{T}}-\frac{1}{2}\left[\ln\left(\frac{p}{p_0}\right)-\frac{S_{H_2}^0}{R}\right]\right\}+1}. \tag{32}$$

This is the central result of our model used to calculate the PTIs.

V. COMPARISON TO EXPERIMENTAL PRESSURE–OPTICAL-TRANSMISSION ISOTHERMS

The present model is applied to pressure–optical-transmission isotherms measured on $Mg_yTi_{1-y}H_x$ gradient thin films. This ensures a reliable comparison of the isotherms, as all compositions y are simultaneously measured under exactly the same pressure and temperature conditions.

The determination of the optical absorption coefficients of the pure Mg and Ti metals is done on separately deposited Pd capped Mg and Ti thin films.[35] The consistency of the results is checked with the data from Palik.[36] The absorption coefficients of the hydrides MgH_2 and TiH_2 are then determined on the same films exposed to 10^5 Pa H_2 pressure. The absorption coefficients of the intermediate Mg_jTi_{4-j} clusters ($j=1,2,3$) are to first order the weighted average of values for pure metals (hydrides).[37] We make use of *ab initio* calculations of the optical properties of Mg-Ti supercells[15] to interpolate more precisely the absorption coefficients (see Fig. 2).

We use the standard molar volumes $V_{Mg}=13.97$ cm^3 (mol)$^{-1}$ and $V_{Ti}=10.64$ cm^3 (mol)$^{-1}$ for the metals. For the hydrides, 32% and 25% volume expansions are assumed for MgH_2 and TiH_2, respectively.[19] Bulk moduli values for the metals are taken as $B_{Mg}=35.4$ GPa, $B_{Ti}=105.1$ GPa,[38] $B_{MgH_2}=50$ GPa,[39] and $B_{TiH_2}=161$ GPa for the hydrides.[40]

Figure 3(a) displays a calculated PCI and its corresponding PTI obtained with the multisite lattice gas model with a realistic set of parameters for a wide range of pressure. In the PCI, the wide distribution of site energies and site fractions results in a gradual increase of the hydrogen concentration with pressure. In comparison, most of the optical-transmission change occurs in a narrower pressure range in the PTI than in the PCI. The high optical absorption coefficient difference of Mg-rich clusters is responsible for this behavior, giving extra weight in transmission to the filling of Mg_4 and Mg_3Ti sites. Similarly, the filling of Ti_4 sites results in an initial decrease of the optical transmission as a consequence of the negative absorption coefficient difference for these sites (see Fig. 2). To put in evidence the contribution of the different sites to the isotherms, the derivative of the concentration and of the optical transmission with respect to the logarithm of the pressure are calculated and plotted in Fig. 3(b). Five peaks corresponding to the five interstitial sites are clearly seen in the derivatives. Due to the predominant Mg fraction ($y=0.61$) and the positive CSRO parameter ($s=0.4$) chosen for this example, Mg-rich sites are contributing most. This effect is even more pronounced in the $\ln(T)$ derivative because of the high transparency of MgH_2 (see Sec. IV F).

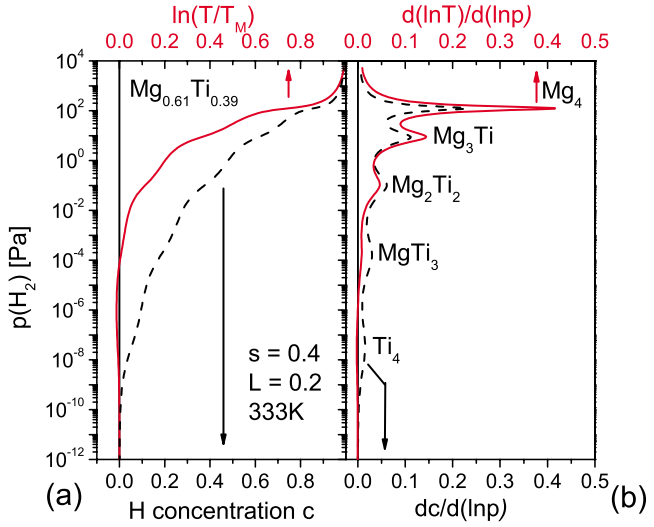

FIG. 3. (Color online) (a) Comparison between PCI (dashed line) and PTI (full line) of $Mg_{0.61}Ti_{0.39}H_x$ at $\mathcal{T}=333$ K as calculated with the multisite lattice gas model with $s=0.4$ and $L=0.2$ (model described in Sec. IV). (b) Derivatives of the H concentration c (dashed line) and of $\ln(T)$ (full line) with respect to $\ln(p)$.

The comparison between modeled and experimental PTIs for five different compositions and three different temperatures is shown in Fig. 4. The solution enthalpies for free Mg_4 (Ti_4) clusters are kept constant *for all compositions and temperatures* at $\Delta H_{Mg}^0=-36.6$ kJ (mol H_2)$^{-1}$ and $\Delta H_{Ti}^0=-85.6$ kJ (mol H_2)$^{-1}$ (see Table I). From XRD measurements, the average $Mg_yTi_{1-y}H_x$ lattice is coherent with no evidence for large-scale phase segregation.[8] Furthermore, since the molar volumes of Mg and TiH_2 are similar, the hydrogenation of Ti-rich sites reduces the differences in volume between clusters and even increases the structural coherence at intermediate hydrogenation stages. The L parameter, which characterizes the local rigidity of embedded clusters with respect to the average lattice, is therefore ex-

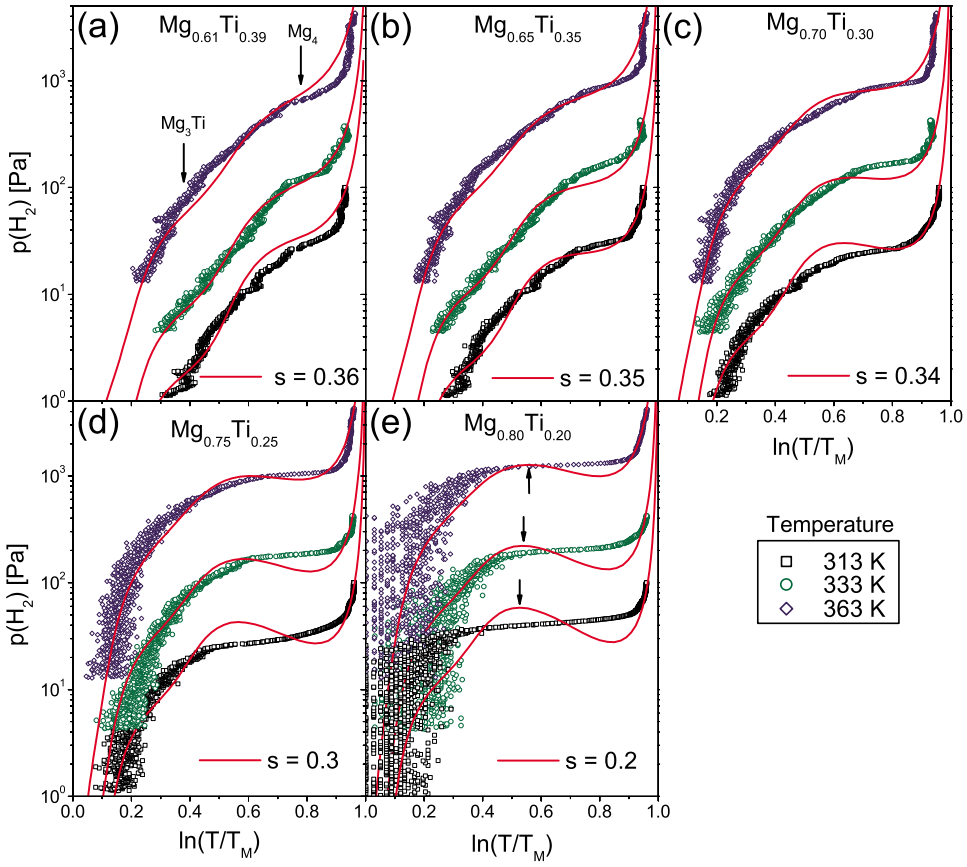

FIG. 4. (Color online) Symbols, [(a)–(e)] experimental pressure–optical-transmission isotherms of $Mg_yTi_{1-y}H_x$ at temperatures $\mathcal{T}$=313, 333, and 363 K and various Mg fractions y. Lines, multisite lattice gas PTI simulations for fixed L=0.2. The chemical short-range order parameter s used for each alloy composition is indicated in the figure. Note that s is independent of temperature. The arrows indicate (a) the transmission at which half of the Mg_3Ti and Mg_4 sites are filled (e) the transmission at the first spinodal concentration (see text).

pected to take a small value: a constant value of L=0.2 gives satisfactory results for all isotherms. The only free parameter for each composition is then the CSRO parameter s.

For every composition $y<0.85$, there is a well-defined positive short-range order parameter value that reproduces the experimental data well for the three temperatures considered. The observed plateau corresponds to the hydrogenation of Mg_4 sites, while the gradual increase of transmission at lower pressure is due to the gradual filling of Ti-containing sites. For high Mg fractions ($y \geqslant 0.75$), the PTIs are reproduced best if assuming a plateau starting near the spinodal concentration, i.e., near the local maximum in the simulated isotherm [see the *arrows* in Fig. 4(e)]. A plateau pressure higher than the one derived by using the Maxwell construction is expected in solid-gas systems where the metal-to-hydride transformation generates coherency strain and therefore adds an additional energy barrier for the phase transformation to proceed.[41,42] The fractions of interstitial sites g_j and the embedded site energies $\Delta H_j^{0,e}$ obtained by modeling as a function of compositions are plotted in Fig. 5. The fraction g_4 of Mg_4 interstitial sites is the largest at all concentrations considered, but for Ti-rich compositions, a significant fraction of all other sites is also present.

It is counterintuitive that for a given temperature, the modeled and experimental plateau pressures *increase* with the Mg fraction y. Indeed, as seen in Fig. 6, the enthalpy of Mg_4 sites decreases with increasing Mg fraction for any fixed H concentration in the hydride, and the plateau pressure should decrease accordingly. However, due to the changing amount of Ti, the minimum concentration $c_{\min}=1-g_4(y)$ at which the Mg_4 site occupation starts is *not* constant. The Mg_4 plateau pressure is thus essentially determined by the enthalpy of Mg_4 sites $\Delta H_4(c_{\min})$ (*stars* in Fig. 6) and slightly increases with increasing Mg fraction. This weak dependence of the Mg_4 site enthalpy on Mg fraction originates from the counteracting effect of the second and third terms in Eq. (25): due to the small size of the Ti atom relative to Mg, alloying makes the second term positive and

TABLE I. Input parameters of the multisite model valid for all compositions y of Mg_yTi_{1-y} and temperatures. The molar volume V in cm^3 $(cm)^{-1}$. The bulk modulus is in GPa. The enthalpy is in kJ $(mol\ H_2)^{-1}$.

V_{Mg}	V_{Ti}	V_{MgH_2}	V_{TiH_2}	B_{Mg}	B_{Ti}	B_{MgH_2}	B_{TiH_2}	ΔH^0_{Mg}	ΔH^0_{Ti}	L
13.97	10.64	18.44[a]	13.30[a]	35.4[b]	105.1[b]	50[c]	162.0[d]	−36.6	−86.6	0.2

[a]Reference 19.
[b]Reference 38.
[c]Reference 39.
[d]Reference 40.

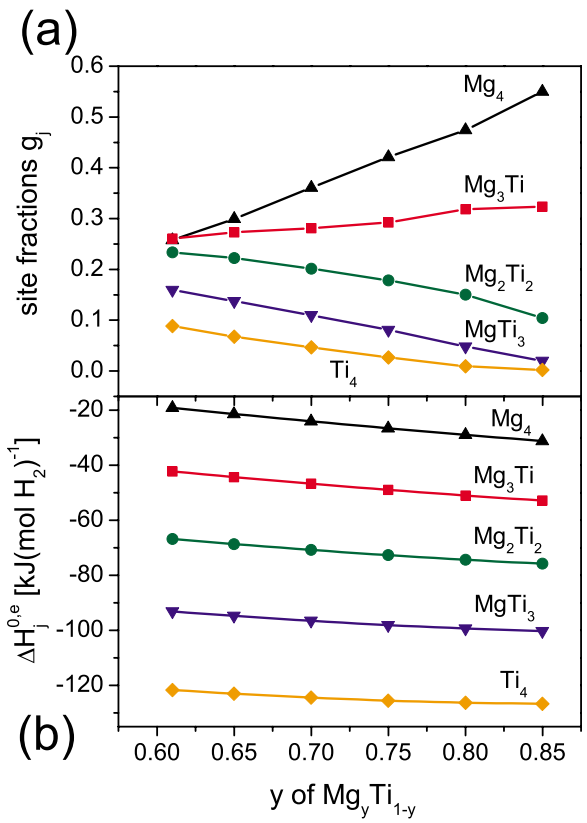

FIG. 5. (Color online) Symbols (a) fractions g_j of Mg_jTi_{4-j} sites and (b) enthalpies of solution per site $\Delta H_j^{0,e}$ derived from the experimental PTIs by using the multisite model described in Sec. IV.

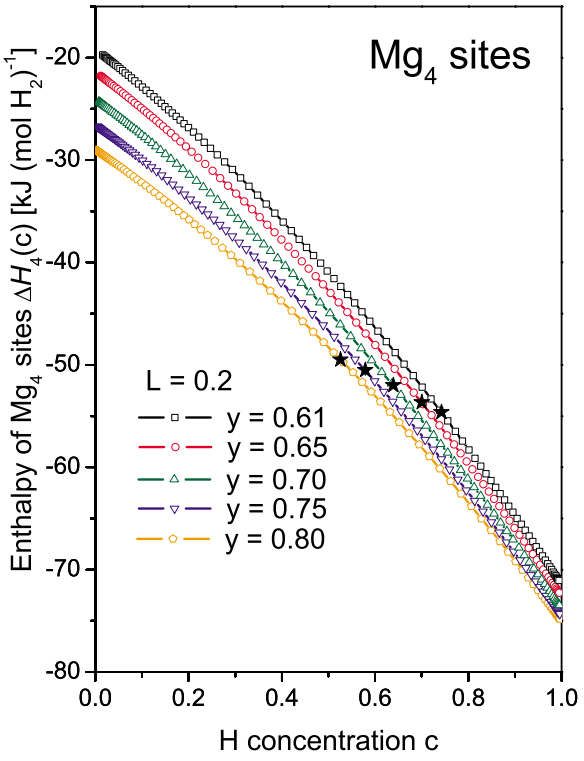

FIG. 6. (Color online) Open symbols, enthalpy of the Mg_4 sites $\Delta H_4(c)$ as a function of H concentration c for various Mg fractions y. Filled stars, enthalpy $\Delta H_4(c_{\min})$ of the Mg_4 sites at the minimum concentration for Mg_4 site occupation $c_{\min}$ as a function of Mg fraction.

reduces the stability of Mg_4 sites toward hydrogen. However, adding Ti also increases $c_{\min}$ and, therefore, destabilizes the hydrogenation of Mg_4 sites via a strengthening of the H-H interaction (third term). These theoretical considerations are consistent with our previous experimental work,[16] where we concluded from the temperature dependence of the Mg_4 site plateau pressure that the Mg_4 enthalpy does not significantly depend on Mg_yTi_{1-y} composition.

VI. DISCUSSION

The input energies used in the modeling [ΔH^0_{Mg} $=-36.6$ kJ (mol H_2)$^{-1}$, $\Delta H^0_{Ti}=-85.6$ kJ (mol H_2)$^{-1}$] are H solution enthalpies and seem at first sight not negative enough. To directly compare the energies used in the modeling with measured hydride (MgH_2 and TiH_2) enthalpies from literature, we need to calculate the enthalpy of a hypothetical material containing only Mg_4 (or Ti_4) sites at half the hydrogen filling ($c=0.5$). For this, we use equation Eq. (25) with $y=1$, $j=4$ (Mg_4 sites) and $y=0$, $j=0$ (Ti_4 sites). The obtained enthalpies are $\Delta H_4(0.5)=-52.2$ kJ (mol H_2)$^{-1}$ and $\Delta H_0(0.5)=-108.6$ kJ (mol H_2)$^{-1}$ for Mg_4 and Ti_4 sites, respectively. These values are ~ 20 kJ (mol H_2)$^{-1}$ less negative than those determined on bulk MgH_2 [$\Delta H=-76$ kJ (mol H_2)$^{-1}$] and TiH_2 [$\Delta H=-130$ kJ (mol H_2)$^{-1}$].[19] Such a discrepancy is not unusual for thin hydride films: due to the hydrogen-induced lattice expansion, films that are clamped to the substrate get strained. Although at high H concentrations dislocations and a complex rearrangement of nanograins reduce clamping effects,[43] the remaining compressive strain reduces the hydride stability in a similar way as alloying does in Eq. (14). For example, experiments on pure Mg thin films report an enthalpy for hydrogen absorption of $\Delta H=-60.7$ kJ (mol H_2)$^{-1}$.[44] Additionally to the clamping to the substrate, the nanostructure of the films can also influence the enthalpy.[45]

To show the sensitivity of the model to the L and s parameters, the isotherms of $Mg_{0.61}Ti_{0.39}$ and $Mg_{0.75}Ti_{0.25}$ at temperature $\mathcal{T}=333$ K are compared to simulations in Fig. 7 with the optimal s parameter and varying L values from completely "soft" ($L=0$) to completely "rigid" clusters ($L=1$) [Figs. 7(a) and 7(c)] and with $L=0.2$, for varying s parameters, from random ($s=0$) to completely segregated Mg_4H_x and Ti_4H_x sites ($s=1$) [Figs. 7(b) and 7(d)].

For constant s and low L values ($L<0.4$), the multisite modeling reproduces the PTIs' shape reasonably well.

For constant s and high L values, the cluster volume goes toward that of free clusters [see Eq. (7)], and the second alloying term in Eq. (25), which effectively separates the site enthalpies $\Delta H_j^{0,e}$ from each other, goes to zero. Consequently, the $\Delta H_j^{0,e}$ values are too close from each other to be discriminated in the isotherms, which therefore exhibit only one large plateau. The gradual increase of pressure with optical transmission experimentally observed is therefore also not reproduced.

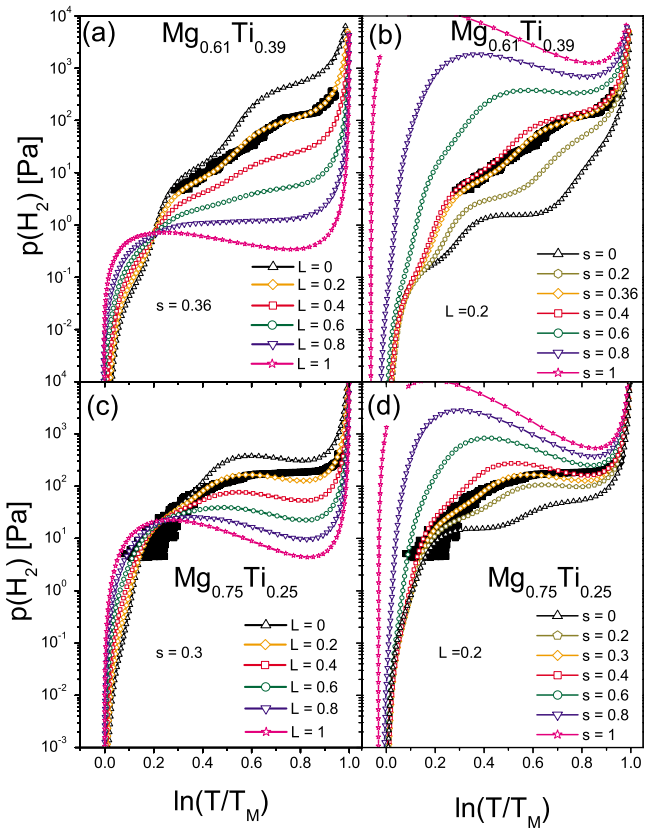

FIG. 7. (Color online) Empty symbols, PTI simulations for $Mg_{0.61}Ti_{0.39}$ with (a) varying L and $s=0.36$ and (b) $L=0.2$ and varying s, and for $Mg_{0.75}Ti_{0.25}$ with (c) varying L and $s=0.36$ and (d) $L=0.2$ and varying s. Filled squares, corresponding experimental pressure–optical-transmission isotherms at temperature $\mathcal{T}=333$ K. The orange diamond symbols are the best simulations, as shown in Fig. 4.

For constant L and a fully random alloy ($s=0$), the Mg_3Ti fraction becomes preponderant and, besides the Mg_4 plateau, a second plateau at lower pressures should be seen in the isotherms. This is not the case in the $Mg_{0.75}Ti_{0.25}$ isotherm and indicates that some local chemical separation occurs in Mg-Ti.

For constant L and fully segregated phases ($s=1$), in this case, only two types of sites exist: Mg_4 and Ti_4. The calculated Mg_4 plateau is the only one in the vicinity of the experimental isotherm and cannot reproduce its sloping behavior.

These examples show that modeling PTIs with a simple multisite lattice gas model is powerful enough to determine s and L parameters and, therefore, discriminate between different possible microstructures in Mg-Ti-H. A certain degree of chemical segregation ($s>0$) must be introduced in the simulated isotherms to properly reproduce the experimental data. Moreover, while the material remains x-ray coherent, the nonzero L parameter shows that the volume of interstitial sites still depends on the local chemical composition and, therefore, indicates the presence of local lattice size modulations. This is consistent with Michaelsen,[46] who showed that coherent inhomogeneities must be larger than several nanometers before they can be detected by conventional XRD.

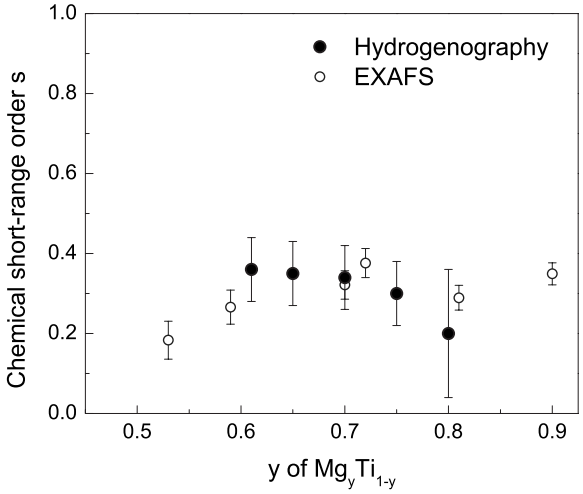

FIG. 8. Filled circles, CSRO parameter s for various Mg_yTi_{1-y} compositions derived from hydrogenography data by means of the multisite model described in Sec. IV. The increased error bar at $y=0.80$ originates from a larger error in the metallic state transmission T_M at this composition. Empty circles, CSRO parameters from EXAFS measurements (as-deposited state, data from Baldi *et al.* (Ref. 20).

According to the model, the successive filling of sites with increasing pressure should result in a modulated isotherm slope [see Fig. 3(b)] and not in a gradual decrease of the isotherm slope, as observed in the experiments [see all panels of Fig. 4]. Within the measured pressure range, two interstitial sites, Mg_3Ti and Mg_4, contribute to the isotherms [see arrows in Fig. 4(a)]. Due to stress and/or microstructural defects, these two interstitial sites most probably have a certain energy distribution for H occupation. This leads to a smearing of the isotherms and, consequently, to a monotonously decreasing isotherm slope.

The values of the CSRO parameter s as a function of composition are summarized in Fig. 8, together with s values obtained from Ti K edge EXAFS measurements.[20] It is remarkable that the values derived from PTI modeling are in such good agreement with those calculated from the first coordination number around Ti atoms determined by EXAFS. In both cases, s is around 0.2–0.4 for Mg fraction $0.6<y<0.8$, with little variation upon composition. This confirms that a certain degree of chemical segregation does occur in systems with a positive enthalpy of mixing, even if a rapid quenching technique such as sputtering is used.

VII. CONCLUSIONS

We use hydrogen as a probe for tracking the degree of chemical segregation in the immiscible $Mg_yTi_{1-y}H_x$ alloy system through the recording and modeling of pressure–optical-transmission isotherms. The unusual shape of the experimental PTIs and the plateau pressures at various Mg atomic fractions y and temperatures are well reproduced by the multisite lattice gas model, assuming the chemical short-range order parameter s as the only free varying parameter. We find that the sloping behavior in the isotherms is repro-

duced assuming the gradual filling with pressure of Ti-containing tetrahedral sites (mainly Mg_3Ti sites in the pressure range measured), while the plateaus are due to the hydrogenation of Mg_4 sites. The CSRO s values derived from the multisite modeling of hydrogenography data agree well with s values determined from EXAFS measurements. The nonzero L parameter shows that the volume of interstitial sites depends on the local chemical composition and, therefore, indicates the presence of local modulations of the crystal lattice size.

The ability to model optical isotherms is a significant step in understanding the hydrogenography results from the microstructural point of view and adds a valuable tool in the combinatorial search for new light-weight hydrogen storage materials. More generally, this multisite lattice-gas model, by determining two essential characteristics of an alloy microstructure that are the CSRO parameter s and the lattice modulation parameter L, is complementary to experimental local-environment probes such as EXAFS or more elaborate modeling approaches using reverse Monte Carlo simulation and molecular dynamics to characterize alloys created between immiscible elements.

ACKNOWLEDGMENT

This work is financially supported by the Stichting voor Fundamenteel Onderzoek der Materie (FOM) through the Sustainable Hydrogen Programme of Advanced Chemical Technologies for Sustainability (ACTS).

*Corresponding author. gremaudr@nat.vu.nl

[1] F. R. de Boer, R. Boom, W. C. M. Mattens, A. R. Miedema, and A. K. Niessen, *Cohesion in Metals: Transition Metal Alloys* (North-Holland, Amsterdam, 1988).
[2] G. Liang and R. Schulz, J. Mater. Sci. **38**, 1179 (2003).
[3] T. Mitchell, S. Diplas, P. Tsakiropoulos, J. F. Watts, and J. A. D. Matthew, Philos. Mag. A **82**, 841 (2002).
[4] R. A. H. Niessen and P. H. L. Notten, Electrochem. Solid-State Lett. **8**, A534 (2005).
[5] P. Vermeulen, R. A. H. Niessen, and P. H. L. Notten, Electrochem. Commun. **8**, 27 (2006).
[6] D. M. Borsa, A. Baldi, M. Pasturel, H. Schreuders, P. Vermeulen, P. H. L. Notten, B. Dam, and R. Griessen, Appl. Phys. Lett. **88**, 241910 (2006).
[7] P. Vermeulen, R. A. H. Niessen, D. M. Borsa, B. Dam, R. Griessen, and P. H. L. Notten, Electrochem. Solid-State Lett. **9**, A520 (2006).
[8] D. M. Borsa, R. Gremaud, A. Baldi, H. Schreuders, J. H. Rector, B. Kooi, P. Vermeulen, P. H. L. Notten, B. Dam, and R. Griessen, Phys. Rev. B **75**, 205408 (2007).
[9] E. Ma, Prog. Mater. Sci. **50**, 413 (2005).
[10] J. H. He and E. Ma, Phys. Rev. B **64**, 144206 (2001).
[11] J. H. He, H. W. Sheng, P. J. Schilling, C.-L. Chien, and E. Ma, Phys. Rev. Lett. **86**, 2826 (2001).
[12] J. H. He, H. W. Sheng, J. S. Lin, P. J. Schilling, R. C. Tittsworth, and E. Ma, Phys. Rev. Lett. **89**, 125507 (2002).
[13] A. Baldi, D. M. Borsa, H. Schreuders, J. H. Rector, T. Atmakidis, M. Bakker, H. Zondag, W. van Helden, B. Dam, and R. Griessen, Int. J. Hydrogen Energy (to be published).
[14] M. Slaman, B. Dam, H. Schreuders, and R. Griessen, Int. J. Hydrogen Energy **33**, 1084 (2008).
[15] M. J. van Setten, G. A. de Wijs, S. Er, and G. Brocks (unpublished).
[16] R. Gremaud, C. P. Broedersz, D. M. Borsa, A. Borgschulte, P. Mauron, H. Schreuders, J. H. Rector, B. Dam, and R. Griessen, Adv. Mater. (Weinheim, Ger.) **19**, 2813 (2007).
[17] R. Gremaud, M. Slaman, H. Schreuders, B. Dam, and R. Griessen, Appl. Phys. Lett. **91**, 231916 (2007).
[18] A. Borgschulte, R. J. Westerwaal, J. H. Rector, B. Dam, and R. Griessen, Appl. Phys. Lett. **85**, 4884 (2004).
[19] *Phase Diagrams of Binary Hydrogen Alloys*, edited by F. D. Manchester (ASM International, Materials Park, 2000).
[20] A. Baldi, R. Gremaud, D. M. Borsa, C. P. Baldé, A. van der Eerden, P. de Jongh, B. Dam, and R. Griessen (unpublished).
[21] R. Lacher, Proc. R. Soc. London, Ser. A **161**, 525 (1937).
[22] R. Griessen and A. Driessen, J. Less-Common Met. **103**, 245 (1984).
[23] H. Hemmes, E. Salomons, R. Griessen, P. Sänger, and A. Driessen, Phys. Rev. B **39**, 10606 (1989).
[24] R. C. Brouwer, J. Rector, N. Koeman, and R. Griessen, Phys. Rev. B **40**, 003546 (1989).
[25] R. C. Brouwer and R. Griessen, Phys. Rev. B **40**, 001481 (1989).
[26] B. E. Warren, B. L. Averbach, and B. W. Robert, J. Appl. Phys. **22**, 1493 (1951).
[27] S. Froyen and C. Herring, J. Appl. Phys. **52**, 7165 (1981).
[28] If available, theoretical values obtained, for example, by means of density functional theory can be used instead of those given by Eq. (10).
[29] R. Griessen and R. Feenstra, J. Phys. F: Met. Phys. **15**, 1013 (1985).
[30] T. Flanagan and J. Oates, in *Hydrogen in Intermetallic Compounds*, Topics in Applied Physics Vol. I, edited by L. Schlapbach (Springer-Verlag, Berlin, 1988).
[31] H. Zabel and H. Peisl, Phys. Rev. Lett. **42**, 511 (1979).
[32] J. D. Eshelby, Proc. R. Soc. London, Ser. A **241**, 376 (1957).
[33] G. Alefeld, Phys. Status Solidi **32**, 67 (1969).
[34] H. Wagner, in *Hydrogen Metals*, Topics in Applied Physics Vol. I, edited by G. Alefeld and J. Völkl (Springer-Verlag, Berlin, 1978).
[35] W. Lohstroh, R. J. Westerwaal, J. L. M. van Mechelen, C. Chacon, E. Johansson, B. Dam, and R. Griessen, Phys. Rev. B **70**, 165411 (2004).
[36] E. D. Palik, *Handbook of Optical Constants of Solids* (Academic, San Diego, 1998).
[37] The weak curvature of the absorption coefficients difference in Fig. 2 shows that if first principles calculation had not been available, a simple linear interpolation would have induced only minor errors. This observation is important for the applicability of our model to alloy system for which experimental (or theoretical) values are not available.

[38] K. A. Gschneider, Solid State Phys. **16**, 308 (1964).
[39] R. Yu and P. K. Lam, Phys. Rev. B **37**, 8730 (1988).
[40] W. Wolf and P. Herzig, J. Phys.: Condens. Matter **12**, 4535 (2000).
[41] R. B. Schwarz and A. G. Khachaturyan, Phys. Rev. Lett. **74**, 2523 (1995).
[42] R. B. Schwarz and A. G. Khachaturyan, Acta Mater. **54**, 313 (2006).
[43] G. Song, M. Geitz, A. Abromeit, and H. Zabel, Phys. Rev. B **54**, 14093 (1996).
[44] A. Krozer and B. Kasemo, J. Less-Common Met. **160**, 323 (1990).
[45] B. Dam, R. Gremaud, C. Broedersz, and R. Griessen, Scr. Mater. **56**, 853 (2007).
[46] C. Michaelsen, Philos. Mag. A **72**, 813 (1995).